BOUNDARY ELEMENT BASED DOSIMETRY METHODS FOR THE ASSESSMENT OF HUMAN EXPOSURE TO RADIATION FROM 5G MOBILE SYSTEMS

DRAGAN POLJAK
FESB, University of Split, Croatia

ABSTRACT

Exposure of humans to 5G mobile communication systems may result in a local surface temperature elevation, i.e. may cause heating skin, ears and eyes. For the frequencies less than transition frequency of 6 GHz the specific absorption rate (SAR) is used to quantify the volume heating. However, according to recently published ICNIRP 2020 safety guidelines, the surface heating above 6 GHz is quantified by absorbed power density (S_{ab}). Furthermore, an alternative dosimetric quantity referred to as transmitted power density (TPD), is also used for internal dosimetry above 6 GHz. This paper aims to review some recently developed internal dosimetry methods based on the use of Galerkin–Bubnov indirect boundary element method for the assessment of human exposure to electromagnetic fields generated by 5G mobile systems. Different tissue models have been used in the paper. Some illustrative computational results have been presented.

Keywords: human exposure, 5G mobile communication systems, electromagnetic-thermal dosimetry, absorbed power density, transmitted power density, boundary element analysis.

1 INTRODUCTION

Local temperature increase at the human body surface is a well-established effect due to exposure to mobile communications systems of fifth generation (5G) [1], [2].

This surface heating is quantified by absorbed power density (S_{ab}) above transition frequency of 6 GHz according to IEEE 2019 and ICNIRP 2020 guidelines [1], [2]. An alternative quantity transmitted power density (*TPD*) can be also used [3], [4]. Note that specific absorption rate (*SAR*) is preferable quantity for frequencies below 6GHz.

This work aims to review recent work of the author on the assessment of S_{ab} and *TPD* in multi-layered tissue exposed to dipole antenna located horizontally to the interface by using boundary element method (BEM).

The assessment of S_{ab}/*TPD* is carried out in three steps:

- The first step in the assessment procedure is to determine the current distribution along the transmitting antenna using the Galerkin–Bubnov indirect boundary element method (GB-IBEM) to numerically handle the Pocklington integro-differential equation (IDE). The influence of the air-tissue interface is taken into account via the corresponding reflection/transmission coefficient.
- The second step is the evaluation of the electric and magnetic field, respectively, generated by the antenna. Provided the current distribution along the antenna is calculated the irradiated fields are determined by numerically calculating the corresponding field integrals by means of BEM formalism.
- The third step is to calculate S_{ab}/*TPD* by integrating radiated electric and magnetic fields according to the definition of S_{ab}/*TPD*.

More mathematical details pertaining to the formulation and related analytical/numerical procedures used to compute S_{ab} /*TPD* have been reported elsewhere, for example, in Poljak et al. [5], [6].

WIT Transactions on Engineering Sciences, Vol 135, © 2023 WIT Press
www.witpress.com, ISSN 1743-3533 (on-line)
doi:10.2495/BE460011

It is worth noting that according to ICNIRP 2020 guidelines S_{ab} is averaged over area of 4 cm^2 and 1 cm^2, respectively, depending on the operating frequency. The two-layer and three-layer tissue models are studied and some illustrative results for S_{ab} and *TPD* are given.

The present paper is organized as follows; Section 2 outlines the Pocklington IDE formulation for the assessment of the current distribution along the antenna, while the definitions for S_{ab} and *TPD* are given in Section 3. Numerical solution method is addressed in Section 4. The results are presented in Section 4, while last section pertains to some concluding remarks.

2 FORMULATION

Geometry of interest is transmitting dipole antenna of length L and radius a positioned parallel to the air-tissue interface (Fig. 1).

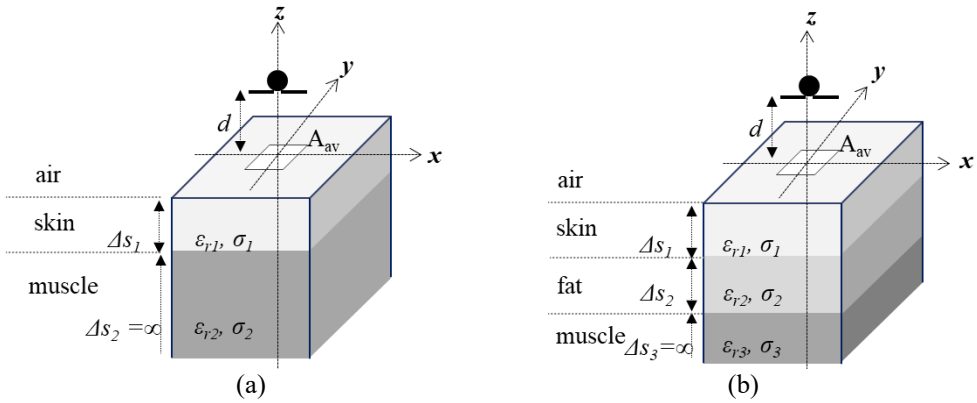

Figure 1: Dipole antenna in front of planar multilayered tissue. (a) 2-layered (SM) model (skin and muscle layers); and (b) 3-layered (SFM) model (skin, fat and muscle).

Fig. 2 shows the propagation of the field radiated from the dipole antenna above the interface through the tissue.

The current distribution $I(x')$ flowing in the axis of straight wire antenna positioned parallel to a multilayered tissue is governed by the Pocklington integro-differential equation [7]

$$E_x^{exc} = j\omega \frac{\mu}{4\pi} \int_0^L I(x')g(x,x')dx' \; - \frac{1}{j4\pi\omega\varepsilon_0} \frac{\partial}{\partial x} \int_0^L \frac{\partial I(x')}{\partial x'} g(x,x')dx', \tag{1}$$

where E_x^{exc} is the electric field tangential to the wire due to an equivalent voltage source and $g(x,x')$ represents the total Green function:

$$g(x,x') = \; g_0(x,x') - \Gamma g_i(x,x'), \tag{2}$$

where $g_0(x,x')$ is the free space-Green function:

$$g_0(x,x') = \frac{e^{-jk_0R_0}}{R_0}, \tag{3}$$

while $g_i(x,x')$ due to the image wire is:

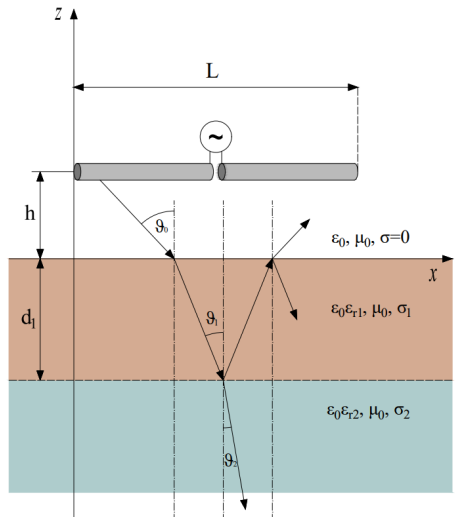

Figure 2: Horizontal dipole antenna in front of planar multilayered tissue.

$$g_i(x,x') = \frac{e^{-jk_0R_i}}{R_i}, \tag{4}$$

where R_0 and R_i are the distances from the source and its image to the observation point of interest, respectively, while k is the phase constant of free space.

The reflection coefficient Γ accounts for the reflection from the interface. More details on the derivation of reflection/transmission coefficient for multilayer structure are available elsewhere, for example, in Poljak et al. [5], [6].

The key point in studying the wire antenna radiation is the assessment of the current distribution. Once the antenna current is calculated, or assumed, it is possible to determine the radiated fields.

Thus, the electric field components are [7]:

$$E_x \frac{1}{j4\pi\omega\varepsilon_{eff}}\left[-\int_0^L \frac{\partial I(x')}{\partial x'}\frac{\partial g(x,y,x')}{\partial x}dx' - \gamma^2\int_{-L/2}^{L/2} I(x')g(x,x')dx'\right], \tag{5a}$$

$$E_y = \frac{1}{j4\pi\omega\varepsilon_{eff}}\int_0^L \frac{\partial I(x')}{\partial x'}\frac{\partial g(x,y,x')}{\partial y}dx', \tag{5b}$$

$$E_z = \frac{1}{j4\pi\omega\varepsilon_{eff}}\int_0^L \frac{\partial I(x')}{\partial x'}\frac{\partial g(x,y,x')}{\partial z}dx', \tag{5c}$$

while the magnetic field components are given by integrals [4]:

$$H_y = \frac{\mu}{4\pi}\int_0^L I(x')\frac{\partial g(x,y,z,x')}{\partial z}dx', \tag{6a}$$

$$H_z = -\frac{\mu}{4\pi}\int_0^L I(x')\frac{\partial g(x,y,z,x')}{\partial y}dx'. \tag{6b}$$

Calculating the electric and magnetic fields in the tissue the dosimetric quantities valid in GHz frequency range (above 6 GHz) can be determined.

3 ABSORBED/TRANSMITTED POWER DENSITY

Dosimetry above 6 GHz requires calculation of absorbed power density (S_{ab}), or the alternative quantity transmitted power density (*TPD*). Definition of S_{ab} and *TPD*, respectively, is given in subsections below.

3.1 Absorbed power density

Widely adopted quantity for the internal dosimetry above 6 GHz according to relevant recently updated guidelines and standards [1], [2] is absorbed power density (S_{ab}) stemming from the generalized conservation law of energy in the electromagnetic field given in the form of Poynting theorem [5] which describes a conservation of the energy stored in electric and magnetic fields within a volume V of interest enclosed by an area A. For the time-harmonic quantities Poynting vector S is

$$\vec{S} = \frac{1}{2} Re\left(\vec{E} \times \vec{H}^*\right), \tag{7}$$

where E and H are the electric and the magnetic field, respectively, due to some source of radiation.

Absorbed pover density S_{ab} adopted in ICNIRP 2020 is defined as [1]

$$S_{ab} = \frac{1}{2A_{av}} \int_{A_{av}} Re\left(\vec{E} \times \vec{H}^*\right) d\vec{A}, \tag{8}$$

where A_{av} is the averaging area, as depicted in Fig. 1.

The choice of averaging area has been addressed in many papers. For example, a circular area of 1 cm^2 has been used in Funahashi et al. [8], while some studies claim that the choice of averaging area of 2 or 4 cm^2 can be correlated with the average mass of 10 g for local SAR [9]. Eventually, Finally, the use of averaging areas of 4 cm^2 and 1 cm^2 has been documented in IEEE [1].

The effect of actual averaging area on *IPD* and S_{ab} due to the Hertz dipole radiation in free space and S_{ab} in the presence of a lossy half-space is available in Poljak and Dorić [10], [11]. More realistic case of dipole antenna above a lossy medium has been recently addressed in Poljak et al. [12].

3.2 Transmitted power density

The transmitted power density (*TPD*) is defined in terms of following integral [6]

$$TPD = \frac{1}{2} \int_0^r \sigma |E(\vec{r})|^2 dr, \tag{9}$$

where r is the variable perpendicular to the body surface and point $r = 0$ pertains to the air-body interface, and σ stands for a tissue conductivity.

4 NUMERICAL SOLUTION

Numerical solution of Pocklington eqn (1) is carried out using GB-IBEM [1] which was documented elsewhere, for example, Poljak [13] and Poljak and El Khamlichi Drissi [14]. The procedure is outlined below.

It is convenient to write (1) in an operator form

$$KI = Y, \tag{10}$$

where K is a linear operator, I is the unknown current to be found for a given excitation E.

GB-IBEM starts by expanding the unknown current $I(x)$ into finite sum of linearly independent basis functions $f_n(x)$ with unknown complex coefficients I_n, i.e.

$$I_n(x') = \sum_{n=1}^{N_g} I_n f_n(x'), \tag{11}$$

where N_g is the number of base functions.

Substituting eqn (11) into eqn (10) one has

$$KI \cong KI_n = \sum_{i=1}^{n} \alpha_i KN_i = Y_n = P_n(Y) \cdot \tag{12}$$

The residual R is defined as

$$R = \sum_{n=1}^{N_g} I_n K(f_n) - E. \tag{13}$$

In accordance to the inner product of functions in Hilbert function space the error R is weighted to zero with respect to certain weighting functions $\{W_j\}$, i.e.

$$\int_L R \cdot W_m^* dx = 0, \quad m = 1,2,..,N_g, \tag{14}$$

where (*) stands for the complex conjugate.

As K is linear, after some mathematical manipulation and by choosing $W_m = f_m$, (the Galerkin–Bubnov procedure) one obtains the following system of equations

$$\sum_{n=1}^{N_g} I_n \int_L K(f_n) f_m \, dx = \int_L E \, f_m dx, \quad m = 1,2,\dots,N_g. \tag{15}$$

Utilizing the weak formulation [13], [14] and performing the integration by parts one obtains

$$\sum_{n=1}^{N_g} I_n \left[\int_{-L}^{L} \int_{-L}^{L} \frac{df_m(x)}{dx} \frac{df_n(x')}{dx'} g(x,x')dx'dx + k^2 \int_{-L}^{L} \int_{-L}^{L} f_m(x) f_n(x') g(x,x')dx'dx \right] = -j4\pi\omega\varepsilon \int_{-L}^{L} E_x^{inc}(x) f_m(x) dx, \quad m = 1,2,\dots,N_g \tag{16}$$

Eqn (16) is the weak Galerkin–Bubnov formulation of IDE (1) now requiring the basis and weight functions from the class of order-one differentiable functions.

Within the framework of the weak formulation boundary conditions are easily incorporated into the global matrix.

Applying the GB-IBEM algorithm and discretizing the wire leads to the global system of equations in the form of generalized Ohm's law

$$\sum_{i=1}^{M} [Z]_{ji} \{I\}_i = \{V\}_j, \quad j = 1,2,\dots,M \tag{17}$$

where M is the total number of wire segments, $[Z]_{ji}$ is the mutual impedance matrix representing the interaction of the ith source to the jth observation segment, respectively and $\{V\}_j$ is the voltage vector for jth observation segment.

As functions $f(x)$ are required to be once differentiable a convenient choice for the shape of functions over the elements is the family of Lagrange's polynomials:

$$f_1(x) = \frac{x_2 - x}{\Delta x}, \; f_2(x) = \frac{x - x_1}{\Delta x}, \tag{18}$$

where x_1 and x_2 are the coordinates of the segment nodes and $\Delta x = x_2 - x_1$ is the segment length.

Now matrix $[Z]_{ji}$ and vector $\{V\}_j$ are given by

$$\begin{aligned}
[Z]_{ji} &= \int_{\Delta l_j}\int_{\Delta l_i}\begin{bmatrix}\dfrac{df_1(x)}{dx}\dfrac{df_1(x')}{dx'} & \dfrac{df_1(x)}{dx}\dfrac{df_2(x')}{dx'}\\ \dfrac{df_2(x)}{dx}\dfrac{df_1(x')}{dx'} & \dfrac{df_2(x)}{dx}\dfrac{df_2(x')}{dx'}\end{bmatrix} g(x,x')dx'dx \\
&+ k^2\int_{\Delta l_j}\int_{\Delta l_i}\begin{bmatrix}f_1(x)f_1(x') & f_1(x)f_2(x')\\ f_2(x)f_1(x') & f_2(x)f_2(x')\end{bmatrix} g(x,x')dx'dx \\
&= \frac{1}{\Delta x^2}\frac{df_1(x')}{dx'}\int_{x_1}^{x_2}\int_{x_1}^{x_2}\begin{bmatrix}1 & -1\\ -1 & 1\end{bmatrix} g_0(x,x')dx'dx \\
&+ \frac{k^2}{\Delta x^2}\int_{x_1}^{x_2}\int_{x_1}^{x_2}\begin{bmatrix}(x_2-x)(x_2-x') & (x_2-x)(x'-x_1)\\ (x-x_1)(x_2-x') & (x-x_1)(x'-x_1)\end{bmatrix} g_0(x,x')\,dx'dx,
\end{aligned} \tag{19}$$

$$\{V\}_j = -j4\pi\omega\varepsilon\int_{\Delta l_j} E_x^{inc}(x)\begin{bmatrix}f_1(x)\\ f_2(x)\end{bmatrix}dx = -\frac{j4\pi\omega\varepsilon}{\Delta x}\int_{x_1}^{x_2} E_x^{inc}(x)\begin{bmatrix}(x_2-x)\\ (x-x_1)\end{bmatrix}dx, \tag{20}$$

where Δl_i, Δl_j are the widths of ith and jth segments.

The voltage vector can be computed analytically for the case of delta-function source (antenna mode), or the plane wave excitation (scatterer mode). In the antenna mode the voltage vector vanishes outside the feed gap area.

The excitation field is

$$E_x^{inc}(x) = \frac{V_g}{\Delta l_g} \tag{21}$$

where V_g is the feed voltage and $\Delta l_g = \Delta x$ (for convenience) is the feed-gap width.

Using the linear shape functions yields

$$\{V\}_j = -\frac{j4\pi\omega\varepsilon}{\Delta l_g}\int_{x_1=-\frac{\Delta l_g}{2}}^{x_2=\frac{\Delta l_g}{2}}\frac{V_g}{\Delta l_g}\begin{bmatrix}(x_2-x)\\ (x-x_1)\end{bmatrix}dx = -j2\pi\omega\varepsilon V_g\begin{pmatrix}1\\ 1\end{pmatrix}. \tag{22}$$

In the scattering mode for the simple case of normal incidence the wire is excited by the plane wave, i.e.:

$$E_x^{inc}(x) = E_0, \tag{23}$$

and the voltage vector is given by:

$$\{V\}_j = -\frac{j4\pi\omega\varepsilon}{\Delta l}\int_{x_1=-\frac{\Delta l}{2}}^{x_2=\frac{\Delta l}{2}} E_0\begin{bmatrix}(x_2-x)\\ (x-x_1)\end{bmatrix}dx = -j2\pi\omega\varepsilon E_0\Delta l - \begin{pmatrix}1\\ 1\end{pmatrix}. \tag{24}$$

More details on the mathematical description of the method can be found elsewhere, e.g. in Poljak [13].

5 NUMERICAL RESULTS

The results for S_{ab} and *TPD* are presented in this section. The results obtained via numerical approach are compared against analytical results [5], [6]. Frequency dependent electrical parameters for the body tissues are available in ITIS Foundation [15].

Table 1: Frequency dependent parameters of body tissues [15].

	Skin		Fat		Muscle	
f (GHz)	ε_r	σ (S/m)	ε_r	σ (S/m)	ε_r	σ (S/m)
6	34.9	3.89	9.80	0.872	48.2	5.20
10	31.3	8.01	8.80	1.71	42.8	10.6

The first set of results deals with the results for S_{ab} vs distance from the interface for different antenna lengths ($L = \lambda/2$, $L = \lambda/4$ and $\lambda/10$). The operating frequency of the transmitting antenna is $f = 10$ GHz. The control surface is $A = 1$ cm^2 and 4 cm^2, respectively. The results obtained via GB-IBEM are compared to the results obtained via assumed sinusoidal current distribution (Fig. 3).

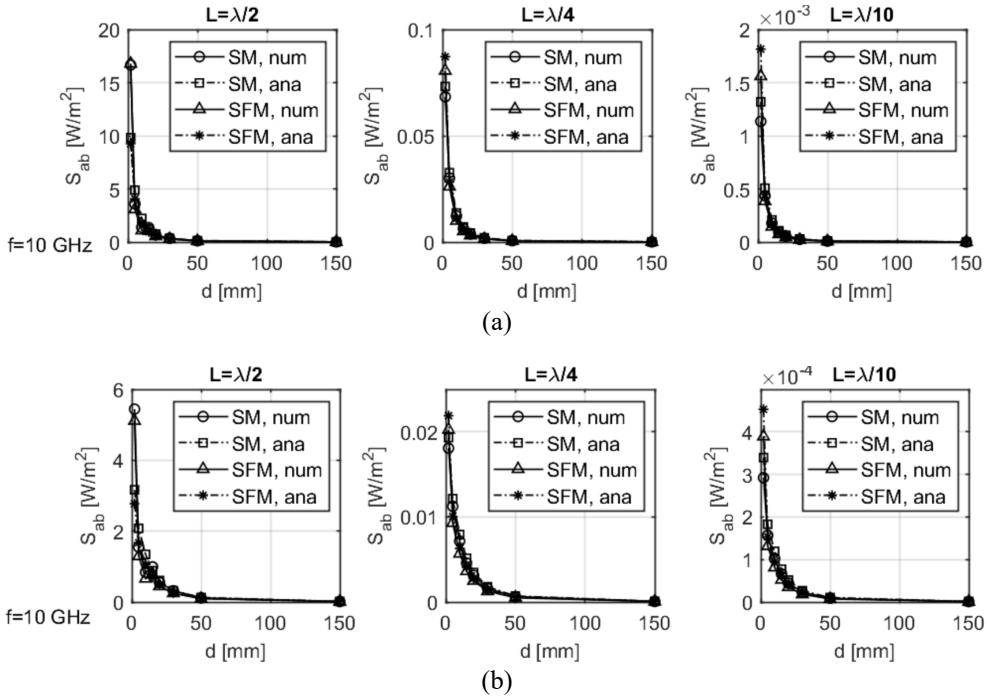

Figure 3: S_{ab} vs antenna-body distance at $f = 10$ GHz for different wire lengths and control surface. (a) $A = 1$ cm^2; and (b) $A = 4$ cm^2.

Discrepancies in S_{ab} values obtained via numerical/analytical approach are approximately, 10% and 20% for wire lengths $L = \lambda/4$ and $\lambda/10$. Also, the discrepancies between SM and SFM models decrease as frequency and antenna-body distance increase.

Fig. 4 pertains to the assessment of *TPD* vs antenna-body distance for different antenna lengths for operating frequency f=10GHz.

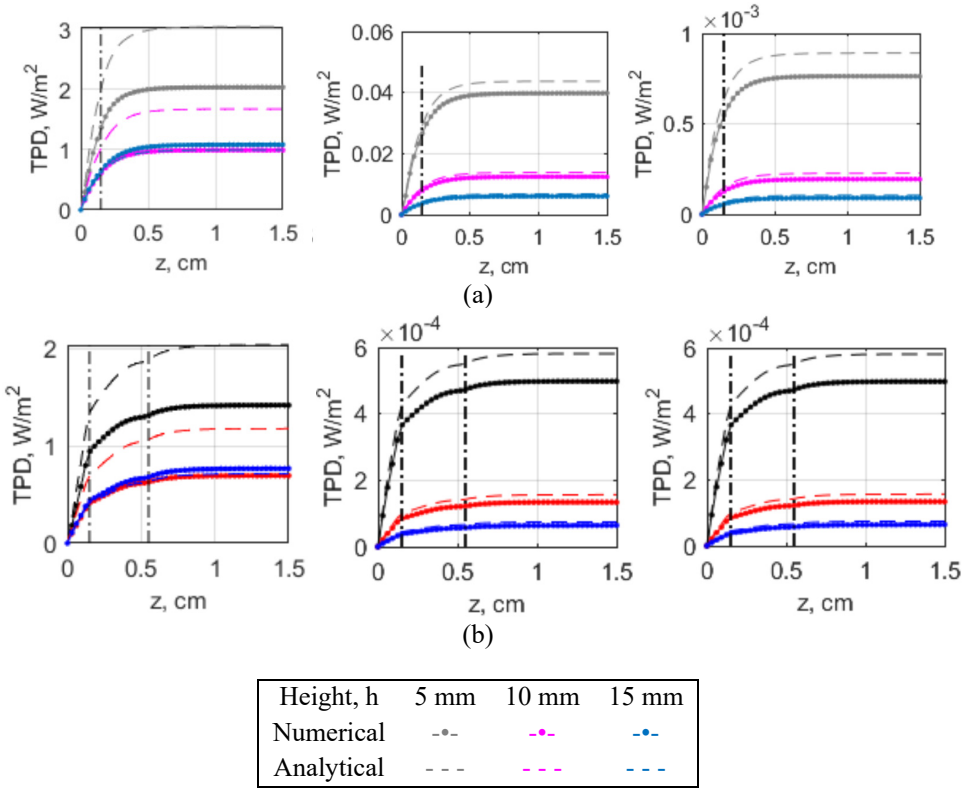

Figure 4: *TPD* versus tissue depth for different antenna lengths ($L = \lambda/2$, $L = \lambda/4$ and $L = \lambda/10$) above multilayered tissue.

TPD obviously grows until saturation rapidly. The discrepancy between analytical/numerical results is highest for $L = \lambda/2$ and increases as antenna-body distance decreases.

6 CONCLUSION

The paper reviews BEM based approaches to determine the dosimetry quantities in GHz frequency range (millimetre waves); absorbed power density (S_{ab}) and transmitted power density (*TPD*) being of interest for 5G mobile systems. Planar two-layer and three-layer tissue models exposed to dipole radiation have been addressed. Some illustrative analytical/numerical results for S_{ab} and *TPD* are given. The obtained results show that S_{ab} decreases rapidly with the increase of the antenna-body distance. The higher is the antenna length, the higher is S_{ab}. Analysing the results for *TPD* it is obvious that the highest

differences between the analytical/numerical results are found for λ/2 dipole. The discrepancy decreases with the antenna length.

REFERENCES

[1] IEEE, IEEE Standard for Safety Levels with Respect to Human Exposure to Electric, Magnetic, and Electromagnetic Fields, 0 Hz to 300 GHz. IEEE Std C95.1-2019 (Revision of IEEE Std C95.1-2005/ Incorporates IEEE Std C95.1-2019/Cor 1-2019), pp. 1–312, 2019.

[2] ICNIRP, Guidelines for limiting exposure to electromagnetic fields (100 kHz to 300 GHz). *Health Physics,* **118**(5), pp. 483–524, 2020.

[3] Pfeifer, S. et al., Total field reconstruction in the near field using pseudo-vector E-field measurements. *IEEE Transactions on Electromagnetic Compatibility,* **61**(2), pp. 476–486, 2019.

[4] Hirata, A., Funahashi, D. & Kodera, S., Setting exposure guidelines and product safety standards for radio-frequency exposure at frequencies above 6 GHz: Brief review. *Annals of Telecommunications,* **74**, pp. 17–24, 2019.

[5] Poljak, D., Susnjara, A. & Kraljevic, L., Assessment of absorbed power density in multilayer planar model of human tissue. *Radiation Protection Dosimetry*, **199**(8–9), pp. 798–805, 2023.

[6] Poljak, D., Susnjara, A. & Fisic, A., Assessment of transmitted power density in the planar multilayer tissue model due to radiation from dipole antenna. *Journal of Communications Software and Systems*, **19**(1), pp. 39–51, 2023. DOI: 10.24138/jcomss-2022-0050.

[7] Poljak, D. et al., Absorbed power density in a multilayer tissue model due to radiation of dipole antenna at GHz frequency range. Part I: Theoretical background. *Proc. Splitech*, Split, Croatia, July, 2022.

[8] Funahashi, D. et al., Area-averaged transmitted power density at skin surface as metric to estimate surface temperature elevation. *IEEE Access,* **6**, pp. 77665–77674, 2018.

[9] Funahashi, D. et al., Averaging area of incident power density for human exposure from patch antenna arrays. *IEICE Transactions on Electronics,* **E101-C**(8), pp. 644–646, 2018.

[10] Poljak, D. & Dorić, V., On the concept of the transmitted field and transmitted power density for simplifed case of hertz dipole. *EMC Europe 2020*, Rome, Italy, 2020.

[11] Poljak, D. & Dorić, V., Assessment of transmitted power density due to hertz dipole radiation using the modified image theory approach. *28th International Conference on Software, Telecommunications and Computer Networks (SoftCOM)*, Split, Croatia, 2020.

[12] Poljak, D., Šušnjara, A. & Džolić, A., Assessment of transmitted power density due to radiation from dipole antenna of finite length. Part I: Theoretical background and current distribution. *29th International Conference on Software, Telecommunications and Computer Networks*, Hvar, Croatia, 2021.

[13] Poljak, D., *Advanced Modeling in Computational Electromagnetic Compatibility*, John Wiley: New York, 2007.

[14] Poljak, D. & El Khamlichi Drissi, K., *Computational Methods in Electromagnetic Compatibility, Antenna Theory Approach versus Transmission Line Models*, John Wiley: New York, 2018.

[15] ITIS Foundation, Copyright © 2010–2021 ITIS Foundation, June 2019. https://itis.swiss/virtual-population/tissue-properties/database/.